

Finite Element Modelling of NiTi Shape Memory Alloy Abutment for an Osseointegration Trans-femoral Implant

W. Xu*

Centre for Biomedical Engineering, Faculty of Engineering and Physical Sciences, University of Surrey, Guildford, Surrey, GU2 7XH, UK

Abstract: Traditionally, prosthetic limb is interconnected to the residual limb via a “socket”. As the body weight upon the prosthesis is transferred through soft tissue to human skeleton, the muscles and skin could be traumatized. To overcome the problem, an osseointegration trans-femoral implant technique has been used to attach prosthetic limb to human skeleton directly. However, due to the malfunction of the prosthetic limb and accidentally loss balance of the prosthetic limb user, a significant impact load could over load the implanted bone. To protect the bone, a shape memory alloy (SMA) abutment was developed. Finite element (FE) method was used to investigate the mechanical performance of NiTi SMA abutments under both static and impact load conditions. In this study, a non-linear FE model was applied to simulate the large deformation of the abutment. The simulation in terms of the maximum stress involved and plastic deformation was used a) for safety and reliability assessment of the abutment, and b) as input for the further study of interfacial stress between femur and implant. A comparison of FE modelling was also made between NiTi SMA and other materials used in the clinical trials. The results reveal that NiTi SMA abutment can release much more impact load and reduce the over stress in the bone significantly.

Keywords: Finite element analysis, Osseointegration implant, Shape memory alloy, Impact loading.

1. INTRODUCTION

For the lower limb amputees, the “socket” type prosthetic limbs are normally used to help the users to regain the walking ability. However, in such a case, the soft tissue of the residual limb has to bear the body weight transfers from the prosthetic limb. As the result of wearing socket type of prostheses, muscles and skin are likely to be traumatized. The greatest contribution of Swedish surgeon P-I Branemark is not only uncovered the osseointegration phenomenon but also made prosperous practice in the oral surgery in past 25 years [1]. His practice demonstrated impressive clinical results of osseointegrated titanium implants in the dental and maxillofacial treatment for over 20 years. A similar technique has been recently extended to orthopaedic applications for attaching prosthetic limb. This technique inserts a titanium implant into the long axis of the principal bone of the residual stump. The distal end of the implant penetrates through the skin of the amputee stump to provide direct limb attachment. This method could overcome the disadvantages of socket type limb attachment. The preliminary clinical trials, conducted principally in Sweden within the Branemark Osseointegration Centre, Gothenburg and consequently Queen Mary’s Hospital in London, have indicated that direct skeletal anchoring of prostheses could be achieved using this kind of percutaneous implants [2]. However, a problem was identified during the clinical trial. Due to the malfunction of the prosthetic limb and accidentally loss balance of the prosthetic limb wearer, a significant impact load could be put on

to the abutment, implant and bone. Five cases have developed a plastic deformation of the implant abutment.

To protect the abutment and bone, a mechanical device was used to reduce the impact load in Sweden. The device was designed to take normal load under a normal condition. At a collision condition, the device functions to absorb impact load when the load is over a certain value. The weaknesses of the device are heavy in weight and low reliability in protection of over bending load. As the result of these limitations, a few cases of the UK clinical trials had developed bent and fractured abutment as shown in Fig. (1).

Shape memory alloys (SMA) have been widely used as actuators [3]. However, in this study, its mechanical damping characteristic was proposed to reduce the impact load on the osseointegration transfemoral implant system. In addition, NiTi SMA has excellent biocompatibility which is essential to the medical application. The MANSIDE project funded by the European Commission within the BRITE-EURAM program was aimed at exploring the potential of SMAs in the field of seismic damping of the civil structures. The results demonstrate that SMA-based damping devices are encouraging [4,5].

Superelasticity is one of the important features of SMAs referring to the high strain recovery ability after a substantial deformation. This is resulted by the stress-induced martensitic transformation. When the stress is released, e.g. the external load is removed, the martensite transforms back into austenite and the specimen returns to its original shape [6,7]. The recoverable strain of SMAs can be as much as 7%, several times more than ordinary metallic alloys without any plastic deformation (rubber-like is a term used for another phenomenon in some SMAs). Superelasticity is, however,

*Address correspondence to this author at the Centre for Biomedical Engineering, Faculty of Engineering and Physical Sciences, University of Surrey, Guildford, Surrey, GU2 7XH, UK; Tel: +44 1483 682368; Fax: +44 1483 306039; E-mail: w.xu@surrey.ac.uk



Fig. (1). Bent and fractured implant abutments.

only observed over a specific temperature. The temperature-dependant character of the superelasticity effect, which is disadvantageous in some other applications, is of less importance in the biomedical field because of the stable temperature of human bodies.

In order to identify the potential advantages of SMA, as a material of the abutment, to damp the impact load upon the osseointegration implant, a non-linear finite element (FE) model was developed based on the tensile testing result of a SMA. The model is used to investigate the mechanical performance of NiTi SMA abutments under a collision load. In this study, the collision force is derived from a clinical X-ray image of the residual limb placed with implant and abutment. The derivation takes account of both plastic and 0.2% elastic deformation of the abutment. With the derived load, FE modelling is carried out using different abutment materials and diameters. In order to proof the basic concept, the simulation is static at this stage, i.e., without taking the strain rate effect due to the latent heat upon the phase transformation into consideration. The discussions over the results of the bone-implant interfacial stress and residual strain in the abutment are made between the simulation of NiTi SMA and commercial pure (CP) titanium.

2. MATERIALS AND METHOD

2.1. Implant and Bone Materials

As an extended part of the osseointegrated implant, Professor Branemark used commercially available pure titanium (CP) for the abutment [8]. The advantage of using CP titanium was to avoid any electro-chemistry and biochemistry mismatching. However, low yield stress of the CP titanium was the major concern of abutment failure under an overloading condition. As an alternative material to replace the titanium, the performance of SMA abutment

titanium, the performance of SMA abutment under the overloading conditions was simulated and compared with titanium abutment by finite element analysis.

Table 1. Mechanical Properties of Titanium (CP)

Properties	Titanium (CP)
Young's Modulus (GPa)	105-110
Yield Strength (MPa)	298
Ultimate Strength (MPa)	426
Density (g/cm ³)	4.5

Table 1 summarises the mechanical properties of commercially available pure titanium (99.6%) used in this study. The values of CP titanium tabulated here were used in the FE analysis. However in order to construct the stress-strain curve which was necessary for the non-linear analysis, some additional parameters were used.

Austenite NiTi SMA generally has suitable properties for surgical implantation. The low elastic modulus of NiTi (which is much closer to the bone elastic modulus than that of any other implant metal) might provide benefits in specific applications. Table 2 summarises the most important mechanical properties of typical NiTi SMAs. It should be noted that the mechanical properties of NiTi SMAs vary with the suppliers and manufacturing processes. As it has been suggested in author's previous study [9, 10], an accurate FE simulation can only be done with the specific mechanical properties of the SMA used.

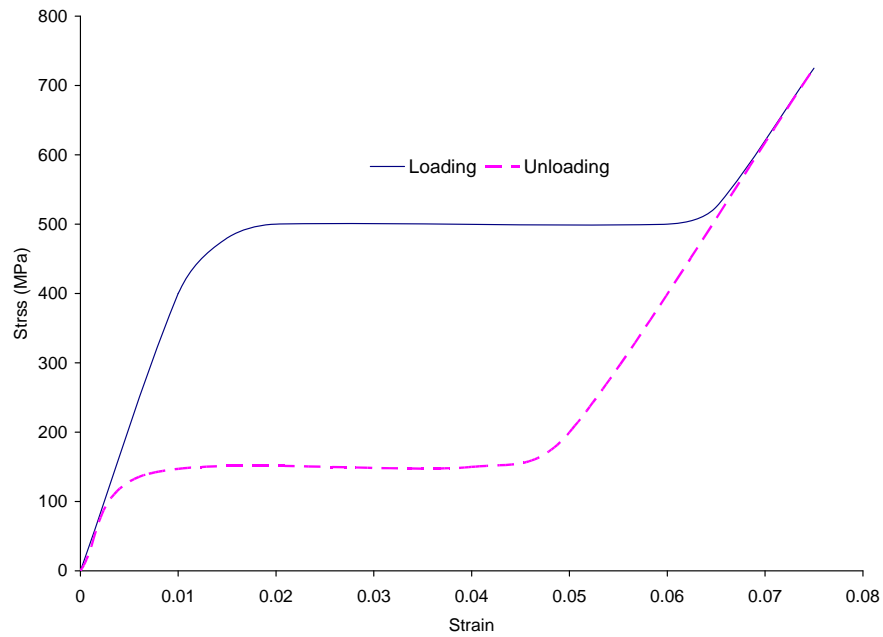


Fig. (2). Tensile strain-stress curve of NiTi.

Table 2. Typical Mechanical Properties of Typical NiTi SMAs

Young's Modulus, E (GPa)	
austenite	83
martensite	28 to 41
Yield Strength, σ_{ys} (MPa)	
austenite	195 to 690
martensite	70 to 140
Poisson's Ratio, ν	
	0.33

In order to obtain an accurate modelling result of non-linear analysis, measured tensile stress-strain curve of a NiTi is used for FE modelling. As shown in Fig. (2), the SMA tensile stress-strain curve consists of loading and unloading two parts in a forward/reverse martensitic transformation cycle. In this study, only the loading part is used, as the purpose of this study is to estimate the effect of collision load to the SMA abutment. For details of non-linear elastic FE modelling of SMAs, one may refer to [8,9].

Bone is among body's hardest parts. Only enamel and dentin are harder. It has unique structural and mechanical properties, which make it suitable for protecting internal organs, facilitating body movement and muscle action. At the macroscopic level bone is composed from two main parts, namely, the cortical or compact bone and the cancellous or trabeculae. Cortical bone always surrounds the cancellous one and has a really dense structure. The cancellous bone is the internal part of a bone, which is composed of trabeculae (thin plates) in a loose mesh structure.

Table 3 lists the mechanical properties of the femur used for this study [11]. It should be noted that bone is not a ho-

mogenous material. In this study, it is assumed that the elastic module of the femur is circumferentially isotropic and behaves linearly through out the strain range of the simulation.

Table 3. Properties of Cortical and Cancellous Human Femur

Young's Modulus, E (GN/m ²)	Cortical	Cancellous
Longitudinal	17.0	0.823
Radial	11.5	0.273
Tangential	11.5	0.273
Poisson's Ratio, ν		
	0.41	0.335

2.2. Determination of the Collision load

In order to find the collision load in deforming the abutment, it was assumed that the deflection of the abutment was caused by point collision between the distal end of the abutment and ground. The permanent deflection of the abutment was the result of perpendicular component of the collision force. The parallel component of the collision force producing compression load to the abutment did not contribute to the deflection. In the course of this study, only the perpendicular force was used.

In order to find out the permanent deformation of the abutment, a patient's X-ray photograph with a deformed abutment was used. 8 mm deformation at the distal end of abutment was identified. This deflected distance was used to calculate the plastic deformation of the abutment. It was assumed that the elastic deformation was fully recovered after the collision. The total deformation strain was obtained by adding 0.2% elastic stain to the plastic strain calculated above.

As the abutment was deformed into a nonlinear plastic range, the collision force was determined by non-linear FE analysis of the deflection process of the abutment. The software used for FE analysis was Ansys 5.6. The Solid 45 element was used for the multi-step transient 3D modelling. The element was defined by eight nodes with three degrees of freedom at each node and has plasticity, creep, swelling, stress stiffening, large deflection, and large strain capabilities.

The abutment model was constrained at one end inserted into the implant by assigning all degrees of freedom of the node to zero. The load applied to the model was the total deflection worked out from both plastic and elastic deformation of the abutment. The non-linear analysis was carried out in an implant-abutment model. This was to determine the collision force.

2.3. Finite Element Modelling of Different Abutment Material

With the collision load derived above, FE simulation was carried out on the whole bone-implant model using two different abutment materials, namely, CP titanium and NiTi SMA. The simulation was static, i.e., without taking the strain rate effect due to temperature increase, resulted by latent heat upon the phase transformation, into consideration. This was because the implanted SMA part was inside of a human body. As such the increase in temperature was rather limited. Furthermore, the static study gave the maximum distortion, which was the most severe case in practice. In order to study the geometrical effect of the abutment, three abutment diameters, 8, 10 and 12 mm were modelled.

To simplify the modelling process, the following assumptions were made in creating the FE models:

- The femur is assumed axi-symmetric and perfectly cylindrical;
- The implant is modelled without threads. It is believed that for the purpose of this study it does not make much difference as the overall strain distribution is of our concern;
- There is a full osseointegration between bone and implant;
- Only the perpendicular force component of the directional load contributed to the deflection of the abutment and the parallel force component was omitted as it only produces compression to the abutment and has no direct effect to the deflection of the abutment.

Same as the above modelling, Solid 45 element was used. The loads were applied in 10 equal subload steps. A number of convergence-enhancement and recovery features, such as line search, automatic load stepping, and bisection, could be activated to help the convergence. In this study, only line search option and predictor were used. It was because the predictor feature accelerates convergence and was particularly useful if the non-linear response was relatively smooth. The materials and abutment diameters of six models are shown in Table 4.

Table 4. Materials and Diameters of FE Models

Model Number	Material	Diameter
Case 1	Titanium	12mm
Case 2	Titanium	14mm
Case 3	Titanium	10mm
Case 4	NiTi	12mm
Case 5	NiTi	14mm
Case 6	NiTi	10mm

3. RESULTS AND DISCUSSIONS

3.1. Results

The collision force to cause the permanent deflection of the abutment is obtained from the FE analysis. The deflection was applied to the node at the distal end of the abutment model. The collision force was obtained from the reaction force on the node where the deflection was applied. The value of collision force was determined as 1822 N. To investigate the effect of the collision force on the abutment and interfacial stress between the bone and implant, von Mises stress and the equivalent strain were used to represent FE modelling results.

A total of six models were evaluated and showed a general pattern with the maximum stress located near to distal femur and the stress near the end part of implant taking a relatively low value with more uniform distribution. Fig. (3) shows typical 3D view of the stress distribution on the implant abutment. Table 5 summarises the maximum values of stress and strain, which occur along the length of the abutment for Cases 1 to 3.

Table 5. Maximum von Mises Stress and Strain Along the Titanium Abutment

Models	Stress (MPa)	Strain
Case 1	428	0.1
Case 2	405	0.07
Case 3	426	0.14

Fig. (4) shows the stress distribution along the abutment for these three cases. Cases 1 and 3 have similar pattern of stress distribution along the abutment, whilst the stress level on the abutment of Case 2 is smaller than the others.

Fig. (5) presents the strain distribution along the abutment for these three cases. It can be seen that all strain curves have similar pattern. Case 3 shows the highest strain, Case 1 has the lowest, and Case 2 is between them. The result also reveals that all three cases have the maximum strain close to the intersection point between the abutment and implant. It is about 70 mm away from the point where the force is applied.

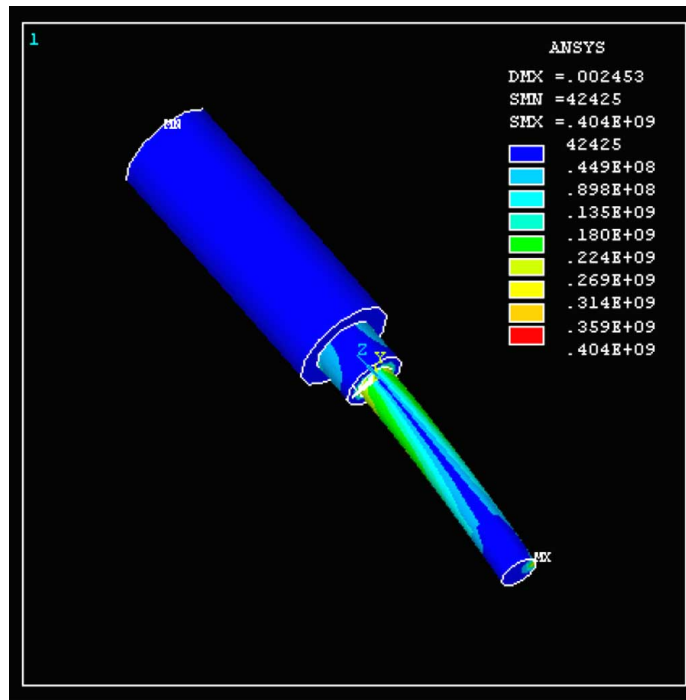


Fig. (3). 3D view of the stress distribution on the implant abutment.

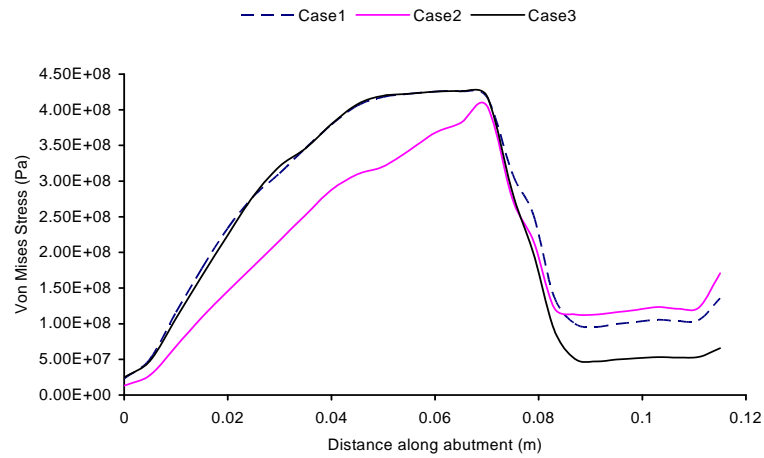


Fig. (4). Von Mises stress along titanium abutment under collision loading.

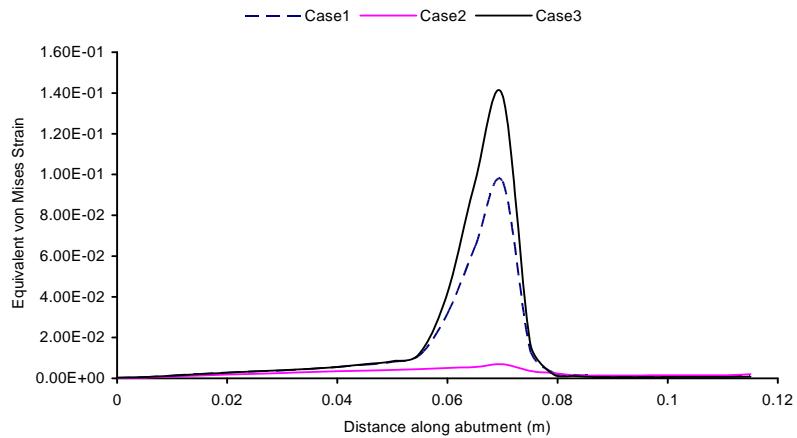


Fig. (5). Von Mises strain along titanium abutment.

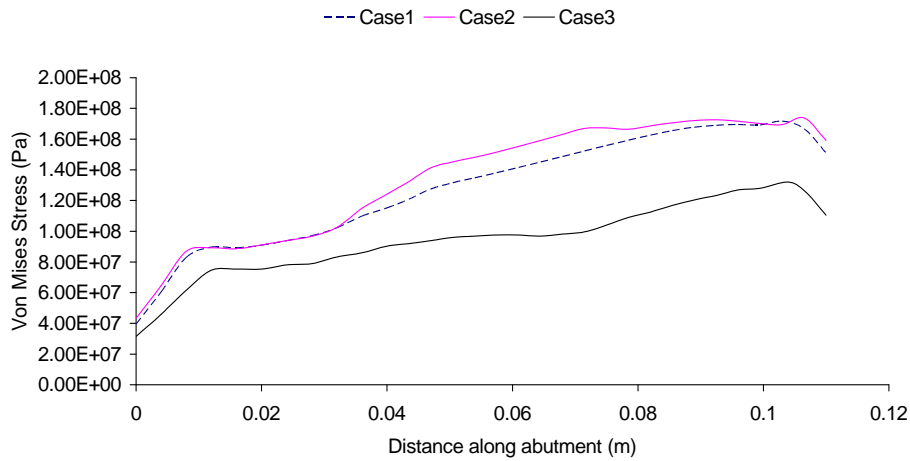


Fig. (6). Von Mises stress distribution at bone-implant interface.

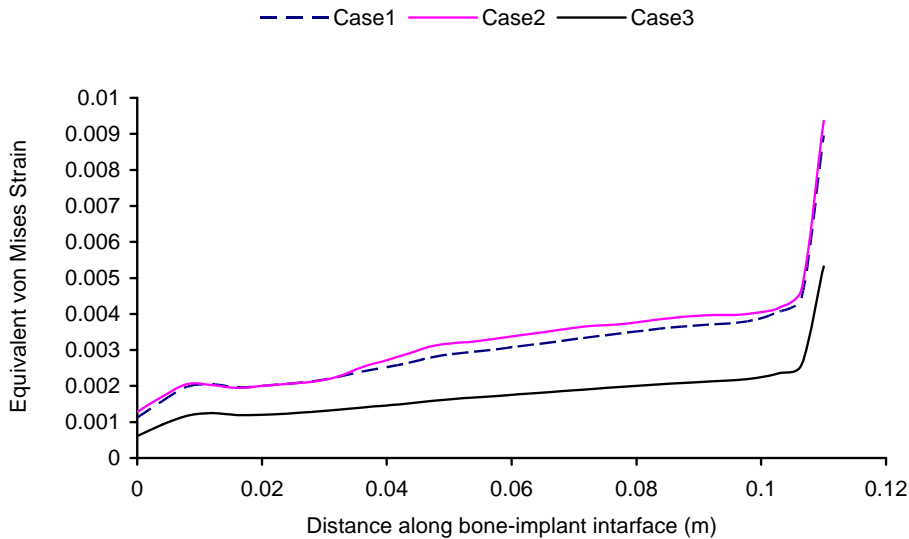


Fig. (7). Von Mises strain distribution at bone and titanium implant.

Table 6 summarises the maximum values of the von Mises stresses and strains of these three cases at the bone-implant interface.

Table 6. Maximum von Mises Stress and Strain at the bone-Implant Interface

Models	Stress (MPa)	Strain
Case 1	172	0.00895
Case 2	174	0.00936
Case 3	132	0.00532

Fig. (6) plots the stress distribution along bone-implant interface of these three cases. It can be seen that Case 2 has stresses along the interface reaching the maximum value of 174 MPa. The result also shows that the stress level of Case 1 is very small.

Fig. (7) shows the strain distribution at the bone-implant interface of these three cases. It can be seen that all strain curves have a similar shape. However the strains of Cases 1 and 2 are very close. Case 3 has the lowest strain.

Table 7 summarises the maximum values of the von Mises stresses and strains along the NiTi abutment of Cases 4, 5 and 6.

Table 7. Maximum von Mises Stress and Strain Along the NiTi Abutment

Models	Stress (MPa)	Strain
Case 4	500	0.05
Case 5	440	0.017
Case 6	725	0.24

Fig. (8) shows the stress distribution along the NiTi abutment for the three different cases. The stress in abutment of Case 5 is the smallest, while Case 6 has the highest overall stress.

Fig. (9) shows the strain distribution along the abutment for the three different cases. It can be seen that all strain curves have similar shapes. Case 6 shows the highest strain level, Case 4 has the lowest strain and the strain of Case 6 is between Cases 4 and 6. Result also reveals that all three

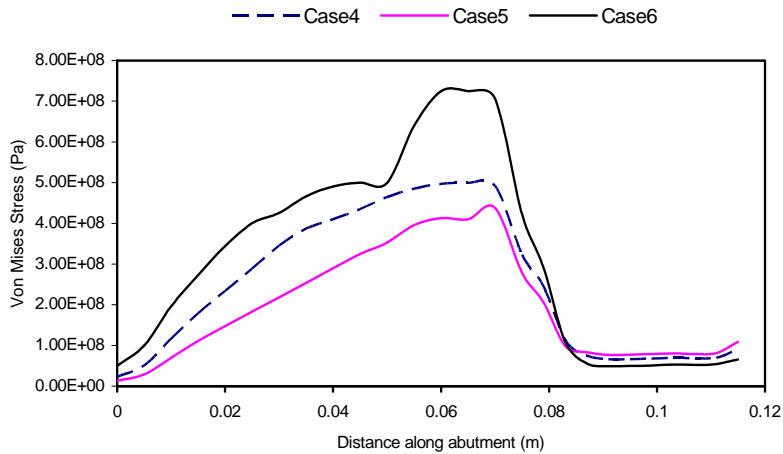


Fig. (8). Von Mises stress along the NiTi abutment.

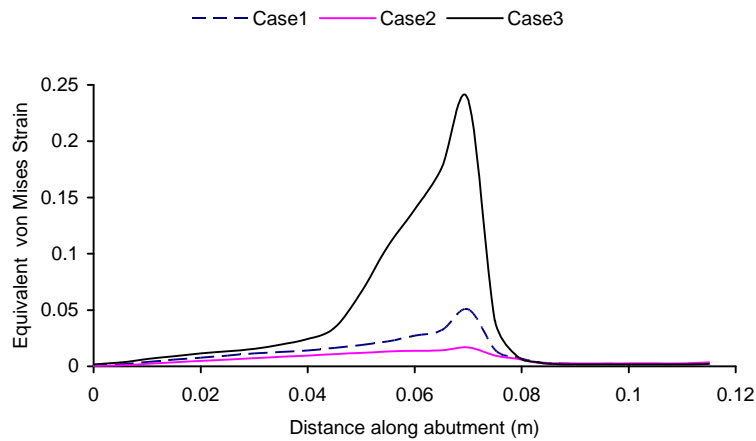


Fig. (9). Von Mises strain along the NiTi abutment.

cases have the maximum strain close to the intersection point between the abutment and implant. It is about 70 mm away from the point where the force is applied.

Table 8 summarises the maximum values of the von Mises stresses and strains of three different cases at the bone-implant interface.

Table 8. Maximum von Mises Stress and Strain at the Bone-Implant Interface

Models	Stress (MPa)	Strain
Case 4	130	0.0097
Case 5	135	0.01
Case 6	118	0.009

Fig. (10) shows the stress distribution along bone-implant interface of three different cases. It can be seen that Case 5 has the maximum stress along the interface of 135 MPa and the stress of Case 1 is very small.

Fig. (11) shows the strain distribution at the bone-implant interface. It reveals that all strain curves have similar shapes. However, the strains in Cases 4 and 5 are very close. Case 6 has the lowest strain.

3.2. Discussions

As the results show, in both titanium and NiTi cases the highest stress along the abutment occurs when the diameter of the abutment is 10 mm. With the increase of the abutment diameter, the stress along the abutment decreases. This agrees with analytical calculations. In all six cases, the case 2 has the lowest stress along the abutment. The general trends of both titanium and NiTi are similar in terms of stress and strain curves. The difference between them is the overall and maximum values along the abutment. For a 12 mm diameter abutment, the maximum stress in NiTi is 17.4% higher than that of Titanium. It is believed that the high stress is because, under the same impact load, the NiTi abutment is deformed more than that of the titanium abutment. The strain level in two relevant models confirms this.

The resultant strains along the abutment reveal that they are influenced more by the material property, i.e., Young’s module, than by the change of the abutment diameter. That is perfectly normal as NiTi is less stiff and can be bent more easily. Apart from the effect of the material property, when the diameter becomes smaller, the response strain increases. Obviously, the combination of those two factors leads to a very high level of strain in Case 6. As the result of this, a high deflection of the implant abutment would occur. A 24% strain has exceeded the maximal recoverable strain of the

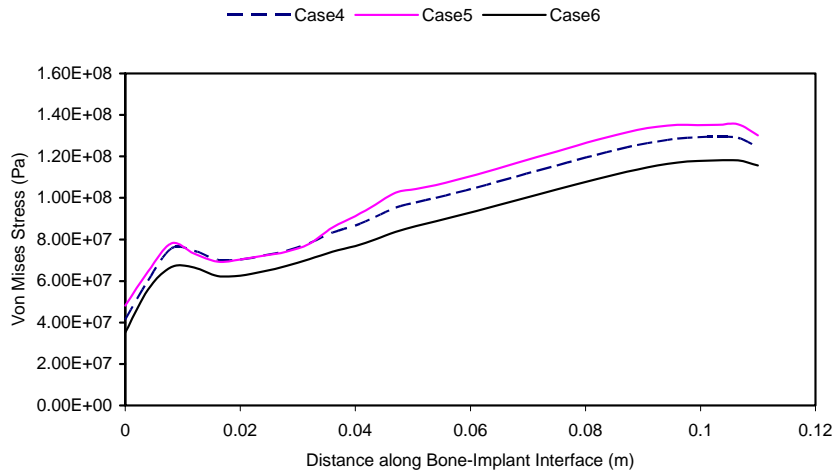


Fig. (10). Von Mises stress distribution at bone and NiTi implant.

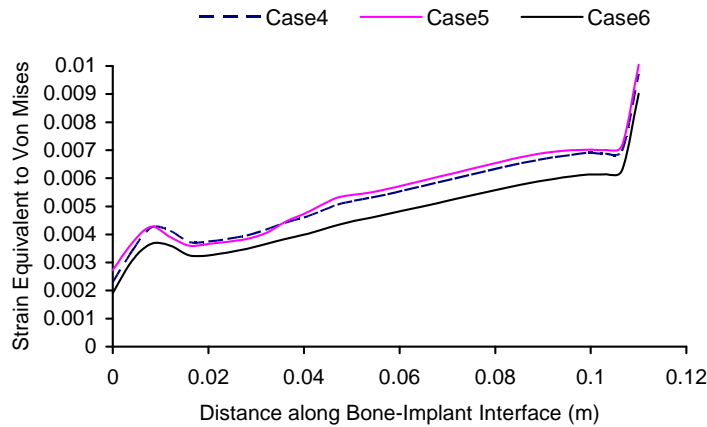


Fig. (11). Von Mises strain distribution at bone and NiTi implant.

NiTi shape memory alloy. Therefore a small diameter TiNi implant would not have any advantage in such a case. However, with small increase of abutment diameter from 10 mm to 12 mm, the strain level decreases significantly to 5%. This is within the recoverable strain level of NiTi SMA (normally below 7%). This indicates if the abutment is working at above the austenite finish temperature, after the overload collision, the abutment is capable to recover back to an unbent shape and continue its service function as before.

The comparison between Fig. (6) and Fig. (10) shows the stress distributions at the bone-implant interface have same pattern but different level. The largest stress along the bone-implant interface occurs in Case 2 where titanium is used. The second highest stress is in Case 1. This model is of the same abutment diameter as used in the clinical trails. The result of NiTi abutment is similar but at a lower stress level. As compared with titanium abutments, under a same overload collision, the maximum interface stress in NiTi abutment is much smaller. The maximum interface stress in Case 4 is 32.3% less than that in Case 1. These results indicate that the stress along the bone-implant interface is largely dependent upon the material and then the diameter of the abutment, i.e., a 10 mm diameter titanium abutment has higher stress than that of a 14 mm diameter NiTi abutment.

The strain distributes along the bone-implant interface in a similar fashion as that of the stress. The highest strain occurs in the NiTi model. The maximum interface strain in the 10 mm NiTi abutment model is higher than that of the 14 mm titanium one. The highest strain is in the case of 14 mm diameter NiTi abutment. A general low level of strain along the interface is observed in the titanium models. However, compared with 32.3% increase in stress, the strain level in the titanium model only reduces by 7.7%.

4. CONCLUSIONS

The main objective of this study was to investigate the stress distribution along the abutment and the bone-implant interface when the prosthetic limb was subject to a collision load. Finite element models with different abutment diameters, namely 10 mm, 12 mm and 14 mm, and two different abutment materials, namely, commercially pure titanium and NiTi SMA, were examined. The following conclusions can be drawn from this study.

As the diameter of abutment increases, the overall stress along the abutment decreases. The general patterns were the same in both NiTi and titanium abutments. For the same abutment diameter, NiTi had higher stress than titanium in the abutment region. Similar behaviour was found in strain distribution. A comparison between two abutment materials

revealed that, for the same abutment diameter of 12mm, NiTi was 32.2% lower in the maximum stress at the bone-implant interface. This suggests that the NiTi abutment would provide better protection to the bone-implant system under the same collision load. However, the stress along the NiTi abutment increased. The result shows, with the same abutment diameter, that the increase in stress in the NiTi abutment was still below the plastic yield stress of the NiTi SMA. The result also revealed that the maximum strain in the 12mm NiTi abutment was 5%. This is below the recoverable strain of the material. The auto recoverable feature was an additional advantage of NiTi abutments. Furthermore, the impact absorption feature of SMAs indicates that NiTi SMA is a suitable material for the abutment.

REFERENCES

- [1] Carr AB, Gerard DA, Larsen PE. The response of bone in primates around unloaded dental implants supporting prostheses with different levels of fit. *J Prosthet Dent* 1996; 76(5): 500-9.
- [2] Branemark R, Branemark PI, Rydevik B, Myers RR. Osseointegration in skeletal reconstruction and rehabilitation: A review. *J Rehabil Res Dev* 2001; 38(2): 175-81.
- [3] Huang WM. On the selection of shape memory alloys for actuators. *Mater Des* 2002; 23: 11-9.
- [4] Dolce M, Cardone D. Mechanical behaviour of shape memory alloys for seismic applications - 2. Austenite NiTi wires subjected to tension. *Int J Mech Sci* 2001; 43(11): 2657-77.
- [5] Dolce M, Cardone D. Seismic protection of light secondary systems through different base isolation systems. *J Earthquake Eng* 2003; 7(2): 223-50.
- [6] Funakubo H, Ed. *Shape Memory Alloys*. New York: Gordon and Breach Science Publishers 1987.
- [7] Duerig TW, Melton KN, Stockel D, Wayman CM, Eds. *Engineering aspects of shape memory alloys*. London: Boston Butterworth Heinemann 1990.
- [8] Sullivan J, Uden M, Robinson KP, Sooriakumaran S. Rehabilitation of the trans-femoral amputee with an osseointegrated prosthesis: the United Kingdom experience. *Prosthet Orthot Int* 2003; 27(2): 114-20.
- [9] Xu W, Frank T, Stockham G, Cuschieri A. Application of finite element analysis to geometrically complicated SMA actuator components. In: Borgmann H, Ed. *Proceedings of the 6th International Conference on New Actuator*; 1998: Bremen, Germany: Messe Bremen GmbH 1998; pp. 1988-93.
- [10] Xu W, Frank T, Stockham G, Cuschieri A. Memory alloy fixator system for suturing tissue in minimal access surgery. *Ann Biomed Eng* 1999; 27: 663-9.
- [11] Xu W, Xu DH, Crocombe AD. 3D finite element stress and strain analysis of a Trans-femoral osseointegration implant. *Proc Inst Mech Eng H* 2006; 220(H6): 661-70.

Received: February 19, 2009

Revised: April 17, 2009

Accepted: April 17, 2009

© W. Xu; Licensee *Bentham Open*.

This is an open access article licensed under the terms of the Creative Commons Attribution Non-Commercial License (<http://creativecommons.org/licenses/by-nc/3.0/>) which permits unrestricted, non-commercial use, distribution and reproduction in any medium, provided the work is properly cited.